Ferroelastic-ferroelectric multiferroics in a bilayer lattice

Ting Zhang, Yan Liang, Xilong Xu, Baibiao Huang, Ying Dai,* and Yandong Ma†
School of Physics, State Key Laboratory of Crystal Materials, Shandong University, Shandanan Street 27, Jinan 250100, China

(Received 21 December 2020; revised 4 March 2021; accepted 12 April 2021; published 23 April 2021)

Two-dimensional multiferroics, combined with ferroelastic and ferroelectric orders, enable unprecedented exploration of applications, such as high-density multistate storage. However, current ferroelastic-ferroelectric-multiferroic research is based on the paradigm of unique symmetry in a single-layer lattice, which restricts ferroelastic ferroelectricity to being rarely explored. Here, going beyond the existing paradigm, we report a design principle for realizing ferroelastic ferroelectricity using the van der Waals interaction as perturbation in a bilayer lattice. Using first principles, we show that, through layer-stacking, bilayer ZrI_2 not only possesses 120° ferroelasticity due to its crystal symmetry but also holds out-of-plane and in-plane polarizations caused by interlayer charge redistribution, thereby achieving ferroelastic-ferroelectric multiferroics in a bilayer lattice. The switch of out-of-plane polarization relates to interlayer sliding, while in-plane polarization reversal correlates with 120° ferroelastic switching. Based on this fact, we propose the six-logic-state multiferroicity. This paper illustrates a tantalizing scheme for achieving and developing two-dimensional ferroelastic ferroelectricity.

DOI: 10.1103/PhysRevB.103.165420

Two-dimensional (2D) multiferroics hosting two or more ferroic orders are of great technological and fundamental importance as they provide a unique opportunity to address multifarious physical effects and potential applications [1–4]. 2D ferroelastic ferroelectricity is one such example. Compared with ferromagnetism which suffers from a low transition temperature in the 2D limit [1,5,6], ferroelasticity and ferroelectricity can sustain relatively higher temperatures as long as the crystal structure is undamaged [7–9]. Meanwhile, ferroelasticity and ferroelectricity are essentially pertinent to crystal structure, and thus the simultaneous existence of ferroelastic and ferroelectric orders in 2D ferroelastic ferroelectricity exhibits a high possibility to be strongly coupled, which is highly useful for practical multiferroic applications [10–12]. This is in sharp contrast with the annoying inherent exclusion between ferroelectricity and ferromagnetism [13] and weak coupling between ferroelasticity and ferromagnetism [14]. These merits, not seen in other multiferroics, have driven huge interest to 2D ferroelastic ferroelectricity.

Currently, 2D ferroelastic-ferroelectric-multiferroic research has been established in the paradigm of crystal-symmetry connected ferroic orders in a single-layer lattice. To facilitate the coexistence of ferroelastic and ferroelectric orders in one single-layer lattice, it requires an extremely stringent crystal symmetry that is not easily accessible. In this case, 2D ferroelastic-ferroelectric multiferroics are rather rare in nature, and their design is shown to be unexpectedly thorny, although both 2D ferroelastics and ferroelectrics independently have been broadly studied in many systems [4,15–19]. Only a few single-layer candidates of 2D ferroelastic ferroelectric multiferroics have been proposed, including 2D BP_5 [8], Bi_2O_2X ($X = S$, Se, Te) [9], GaTeCl [11], AgI [12], and phosphorene analogues [7,10]. This greatly obstructs the further explorations and potential applications of 2D ferroelastic ferroelectricity. It is therefore of fundamental scientific interest to explore a scheme to achieve 2D ferroelastic ferroelectricity, especially with strong ferroelastic-ferroelectric coupling.

In this paper, by studying an example system of bilayer ZrI_2, we present a design principle for realizing 2D ferroelastic-ferroelectric multiferroics in a bilayer lattice. Based on first-principles calculations, our results show that the spontaneous structure polarization induces three distinct orientation states in bilayer ZrI_2, and the van der Waals stacking leads to interlayer charge redistribution. These two effects bring simultaneously the 120° ferroelasticity and bidirectional (in and out of plane) ferroelectricity, realizing the 2D ferroelastic-ferroelectric multiferroics in bilayer ZrI_2. The switch of the resulting out-of-plane polarization is associated with interlayer sliding, while the reversal of in-plane polarization depends on ferroelastic switching. Such strong coupling between ferroelastic and ferroelectric orders produces an extraordinary six-logic-state multiferroicity in bilayer ZrI_2. The explored design scheme and mechanism of ferroelastic ferroelectricity in a bilayer lattice not only are useful for fundamental research in 2D ferroelastic-ferroelectric multiferroics but also enable a wide range of applications in nanodevices.

Our calculations based on density functional theory were carried out by using the Vienna *ab initio* Simulation Package [20]. The generalized gradient approximation parametrized by Perdew, Burke, and Ernzerhof [21,22] was adopted for the exchange correlation. A vacuum thickness of 30 Å along the *c* direction was introduced to avoid spurious interactions

*Corresponding author: daiy60@sina.com
†yandong.ma@sdu.edu.cn

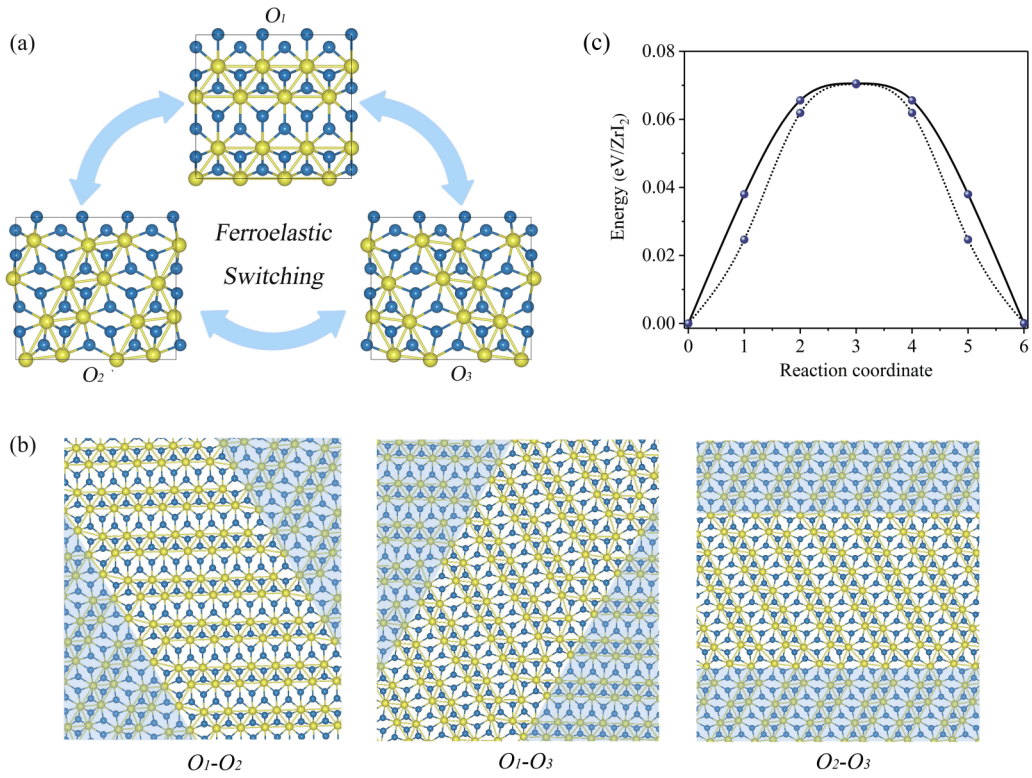

FIG. 1. (a) Schematic diagram of ferroelastic switching among the three different orientation states of monolayer ZrI_2. (b) Ferroelastic domain boundaries between different orientation variants. The domains of different orientations can coexist and form domain boundaries, which we refer to as O_1-O_2, O_1-O_3, and O_2-O_3, respectively. The domains of different orientations are distinguished by different colors. (c) Energy barrier of the most effective ferroelastic switching based on the nudged elastic band (NEB) method for monolayer (dotted line) and bilayer (full line) ZrI_2.

between neighboring sheets. A Monkhorst-Pack k-point mesh of $11\times7\times1$ was utilized. The kinetic cutoff energy was set to 500 eV. Structures were fully relaxed with convergence criteria of 10^{-5}eV and 0.01 eV/Å for energy and force, respectively. The van der Waals interaction was accounted for by using the Grimme's DFT-D3 method [23]. *Ab initio* molecular dynamics (AIMD) simulations were performed on a canonical ensemble with a Nosé thermostat at 300 K for 5 ps with a time step of 1 fs [24]. The phonon dispersion was based on a supercell approach using PHONOPY code [25]. The energy barriers were investigated using the nudged elastic band (NEB) method [26]. The ferroelectric polarization was calculated using the Berry phase approach [27], and the dipole correction was adopted to meet the convergent criterion [28].

The ferroelastic phase usually originates from a structural phase transition (or a hypothetical one) that reduces the symmetry of a prototype one [4]. Compared with the "flexible" ferroelectricity that results from the separation between positive and negative charges [29], undoubtedly, ferroelasticity is "stubborn," which is hard to be generated through external methods. To design or search for 2D ferroelastic-ferroelectric multiferroics, ferroelasticity must be first satisfied. The stubborn character of ferroelasticity, on the contrary, is also a merit superior to ferroelectricity, as it will be robust against external perturbations to some extent. Then if we further introduce nonequivalence into the structure using perturbations, which breaks the charge distribution balance, electric polarization occurs. In this case, the appearance of 2D ferroelastic-ferroelectric multiferroics might be expected. We find this scenario can be realized using the van der Waals interaction in a bilayer lattice.

One candidate system to study this design principle is ZrI_2. Bulk ZrI_2 [30,31] has been known, which features a van der Waals layered structure ($Pmn2_1$ symmetric group). Figure 1(a) shows the crystal structure of monolayer ZrI_2, wherein two adjacent lines of Zr atoms dimerize and form parallel chains. In view of the particular structure symmetry of P_{21}/m, the dimerization of adjacent parallel lines of Zr atoms could occur along three equivalent directions [i.e., $o_1 = \hat{a}$, $o_2 = -\frac{1}{2}\hat{a} - \frac{\sqrt{3}}{2}\hat{b}$, and $o_3 = -\frac{1}{2}\hat{a} + \frac{\sqrt{3}}{2}\hat{b}$], which generates three orientation states. For convenience of discussion, we refer to the three orientation states as O_1, O_2, and O_3, respectively. These three orientation states are related to each other by a rotational symmetry operation of $\{\frac{1}{3}|abc\}$. According to the crystal symmetry, these three orientations can construct three different ferroelastic domain boundaries. Note that the sizes of ferroelastic domains are generally in the order of nanometers [32–36], we take the supercell containing about 100 atoms (∼5 nm) to construct ferroelastic domains, as shown in Fig. 1(b). The formation energy of ferroelastic domains is 16.3 meV/Å, which is close to that of T′-TMDs (27–52 meV/Å) [4], facilitating the formation of the domains.

Under an external stimulus, these three orientations can be converted to each other, thus realizing a 2D tristate ferroelasticity in monolayer ZrI_2. Taking the O_1 and O_2 states as

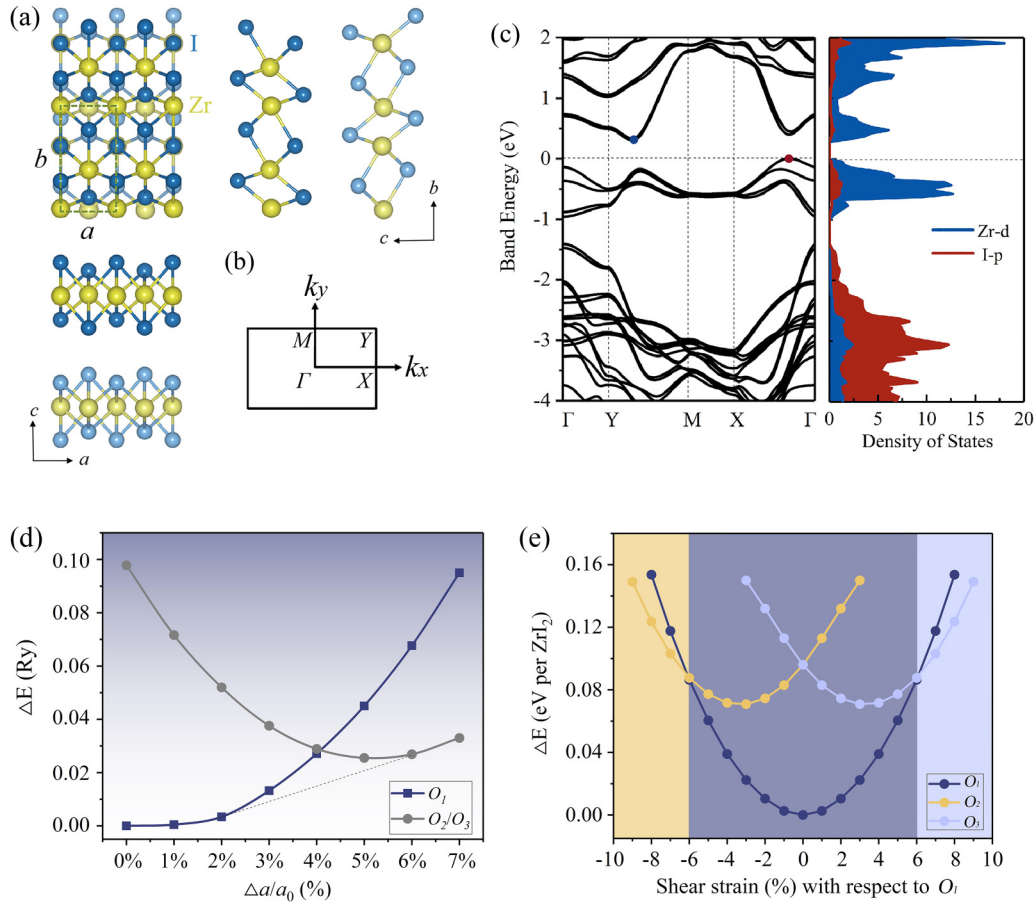

FIG. 2. (a) Crystal structure of bilayer ZrI_2 from top and side views. (b) The two-dimensional (2D) Brillouin zone for bilayer ZrI_2. (c) Band structures and projected density of states of bilayer ZrI_2. The Fermi level is set to zero. The energy profiles of three different orientation states of bilayer ZrI_2 as a function of (d) uniaxial and (e) shear strains. The dashed line in (d) is the common tangent between the two curves.

representatives, we calculate the pathway and energy barrier for the ferroelastic switching employing the NEB method. It is found that the energy barrier against direct shifting of the O_1 to the O_2 state via the paraelastic state is 0.4 eV/f.u., as illustrated in Fig. S1(a) in the Supplemental Material [37]. The inset in Fig. S1(a) in the Supplemental Material [37] shows the crystal structure of the paraelastic state with the space group $P\bar{3}m1$. The phonon spectra of the paraelastic state exhibit obvious imaginary frequencies, which reveals that the paraelastic state is unstable, as can be seen from Fig. S1(b) in the Supplemental Material [37]. The paraelastic state would experience a spontaneous symmetry breaking, resulting in three equally stable orientation states due to its threefold axis. Fortunately, there is an alternative process with a significantly lower barrier to switch from the O_1 to the O_2 state, which does not include the paraelastic state, as shown in Fig. S2 in the Supplemental Material [37]. The overall energy barrier of this process is much lower, with the highest barrier only 0.07 eV/f.u.; see the dotted line in Fig. 1(c).

Upon van der Waals stacking, obviously, bilayer ZrI_2 with space group Pm (No. 6) will inherit the characteristic ferroelasticity [Fig. 2(a)]. Then we calculate the energy barrier of the ferroelastic switching in bilayer ZrI_2; see the full line in Fig. 1(c). The switching barrier is found to be 0.07 eV/f.u., not much different from the barrier of monolayer ZrI_2. This value is smaller than those of single-layer phosphorene [7], GaTeCl [11], borophane [38], and 1T′-WTe_2 [4], but larger than that of $BaTiO_3$ whose Curie temperature is >400 K [7,39]. Therefore, bilayer ZrI_2 is expected to retain its ferroelastic switching capability beyond room temperature, suggesting the in-plane ferroelasticity is robust against the perturbation of the van der Waals interaction in bilayer ZrI_2.

To get better insight into the ferroelasticity of bilayer ZrI_2, we describe the ferroelastic transition process mathematically using 2×2 in-plane transformation strain matrixes. The three orientation states of bilayer ZrI_2 are based on 2×2 supercells. According to the equilibrium lattice vectors and the relaxed atomic coordinates in Cartesian coordinates, the supercell matrices corresponding to the O_1, O_2, and O_3 states of bilayer ZrI_2 are constructed as: $H_1 = (7.492, 0; 0, 13.711)$; H_2=(7.808, −0.333; −0.073, 13.164); H_3=(7.808, 0.333; 0.073, 13.164). These three supercell matrices are connected with each other by the transformation matrix J_{ij}, namely $H_j = J_{ij}H_i$. The transformation strain matrix η_{ij} can then be obtained with J_{ij} based on the Green-Lagrange strain tensor [4,11]:

$$\eta_{ij} = \tfrac{1}{2}\left(J_{ij}^T J_{ij} - I\right) = \tfrac{1}{2}\left[\left(H_i^{-1}\right)^T H_j^T H_j H_i^{-1} - I\right],$$

where T represents matrix transpose, and I denotes a 2×2 identity matrix. The transformation strain matrix η_{ij} has a symmetric form (ε_{aa} ε_{aa}, ε_{ab}; ε_{ab}, ε_{bb}), where ε_{aa} (ε_{bb}) is the tensile (compressive) strain along the a (b) direction, and ε_{ab} is the shear strain component. Here, we use O_1 state as a reference state and obtain the transformation strain matrices associated with $O_1 \rightarrow O_2$ and $O_1 \rightarrow O_3$ switching in bilayer ZrI_2 as follows:

$$\eta_{12(O_1\rightarrow O_2)} = \begin{pmatrix} 0.043 & -0.017 \\ -0.017 & -0.039 \end{pmatrix},$$

$$\eta_{13(O_1\rightarrow O_3)} = \begin{pmatrix} 0.043 & 0.017 \\ 0.017 & -0.039 \end{pmatrix}.$$

This indicates that the O_2 (O_3) state becomes thermodynamically more favorable than the O_1 state with imposing an external strain of magnitude η_{12} (η_{13}) on the O_1 state in bilayer ZrI_2. It is therefore conceivable to apply an external strain to switch these three orientation states of bilayer ZrI_2.

To study in detail the relative energetic stability between these different orientation states of bilayer ZrI_2 under external mechanical deformations, we calculate the energy profiles as a function of uniaxial and shear strains. We take the equilibrium O_1 state as reference, and set the O_2 and O_3 states with the same dimension of the O_1 state along the a direction. The uniaxial strain is imposed along the a direction, and the stress along the b direction is relaxed. The corresponding results are shown in Fig. 2(d), wherein we can draw a common tangent between the energy curves of the O_1 and O_2/O_3 states, with the intersection points being 2 and 6%. Upon imposing the uniaxial strain within the range of 2–6%, the O_1 state tends to reduce its free energy by coexisting with the O_1 and O_2/O_3 states [4], which suggests that the transition from the O_1 to O_2/O_3 states is expected to occur. As shown in Fig. 2(d), the O_2 and O_3 states are energetically degenerate under the uniaxial strain, which can be attributed to the fact that homogeneous uniaxial strain cannot break their mirror symmetry along the b direction. Figure 2(e) shows the energy profiles as a function of shear strain. O_3 and O_2 become the lowest-energy states for bilayer ZrI_2 when the shear strain imposed on the O_1 state reaches 6 and -6%, respectively, making these three orientation states distinguishable and switchable. Accordingly, to realize the reversal switching between these three ferroelastic orientations, namely, achieving tristate ferroelasticity, in bilayer ZrI_2, shear strain should be considered.

As we mentioned above, ferroelectricity stems from the separation between positive and negative charges caused by symmetry breaking. Monolayer ZrI_2 possesses a C_{2h} point group with a mirror plane symmetry M_a perpendicular to the a direction and a twofold screw rotation symmetry C_{2a}, forming an inversion symmetry M_aC_{2a} or $C_{2a}M_a$. In this regard, electric polarization cannot be expected in monolayer ZrI_2. Upon introducing the perturbation of the van der Waals interaction into bilayer ZrI_2, the mirror plane symmetry M_a is preserved, while the C_{2a} symmetry is broken, although the stubborn ferroelasticity is demonstrated to be robust against this perturbation. As a result, bilayer ZrI_2 belongs to the C_s point group and, obviously, exhibits neither mirror symmetry nor inversion symmetry in the c and b directions. The absence of inversion symmetry in the c and b directions will break their charge distribution balances, and thus the out-of-plane and in-plane electric polarizations might be expected in bilayer ZrI_2. Figure S3 in the Supplemental Material [37] shows the structure and the phonon spectra of the paraelastic-paraelectric state (space group $Pm1$) of bilayer ZrI_2, from which we can see pronounced negative frequencies. This indicates the instability of the paraelastic-paraelectric state of bilayer ZrI_2, which would experience spontaneous transformation into the ferroelectric-ferroelastic states. This is consistent with the theory of ferroelectric and ferroelastic phase transitions [40–42]. The symmetry of bilayer ZrI_2 is the same as in the bulk crystal. In addition, compared with bilayer ZrI_2, bulk ZrI_2 (space group $Pmn2_1$) has an additional symmetry element, namely, diagonal glide plane $\{M_b|\frac{1}{2}0\frac{1}{2}\}$. Thus, the difference between bulk and bilayer ZrI_2 is that the former has only out-of-plane polarization but no in-plane polarization.

To verify this assumption, we investigate its electric polarizations along the c and b directions using the Berry phase approach. As expected, our calculations show that bilayer ZrI_2 simultaneously presents the out-of-plane and in-plane electric polarizations of 2.1×10^{-4} and 9.4×10^{-4} C/m^2, respectively. These polarizations are comparable with that of bilayer WTe_2 (3×10^{-4} C/m^2) [43,44] and smaller than those of $BaTiO_3$ (3×10^{-2} C/m^2) [45,46], 1T-MX_2 ($M = Mo$, W; $X = S$, Se, Te) (1.0×10^{-3} to 2.3×10^{-3} C/m^2) [47], Sc_2CO_2 (1.0×10^{-2} C/m^2) [48], and FeO_2H (0.68×10^{-10} C/m) [49]. The out-of-plane and in-plane electric polarizations in bilayer ZrI_2 can also be confirmed by the differential charge density and plane-averaged electrostatic potential analyses. As shown in Fig. 3(d), one can see an apparent charge transfer from the bottom to the top layer, suggesting a spontaneous out-of-plane electric polarization pointing downward. Figure S4(a) in the Supplemental Material [37] gives the plane-averaged electrostatic potential along the c direction. The appearance of a positive discontinuity ($\Delta V = 0.03$ eV) between the vacuum levels of the top and bottom layers indicates the charge transfer from the bottom to the top layer, further confirming the out-of-plane electric polarization, while for the case in the b direction, the different charge density and plane-averaged electrostatic potential also display obvious asymmetry, establishing a spontaneous in-plane polarization [see Figs. 3(e) and S5 in the Supplemental Material [37]]. Therefore, by introducing the perturbation of the van der Waals interaction, the out-of-plane and in-plane electric polarizations are achieved in bilayer ZrI_2.

The existence of spontaneous electric polarizations does not guarantee ferroelectrics unless the electric polarizations are switchable. Then we first study the switching of the out-of-plane electric polarization in bilayer ZrI_2. We define the state with electric polarization along the $-c$ direction as *state-1* [Fig. 3(a)] and the other energetically degenerate state with electric polarization along the c direction as *state-2* [Fig. 3(b)]. The two states are the most stable configuration for bilayer ZrI_2 (see Fig. S6 in the Supplemental Material [37]). In *state-1*, the horizontal distance $-b_1$ ($-b_2$) between I3 (I4) and I1 (I2) is found to be -0.76 Å (-0.73 Å); and in *state-2*, the horizontal distance b_2 (b_1) between I1 (I2) and I3 (I4) is 0.73 Å (0.76 Å). Under a slight interlayer sliding of $b_1 + b_2 = 1.49$ Å along the b direction, the *state-1* can be transformed into *state-2* and vice versa, which provides a

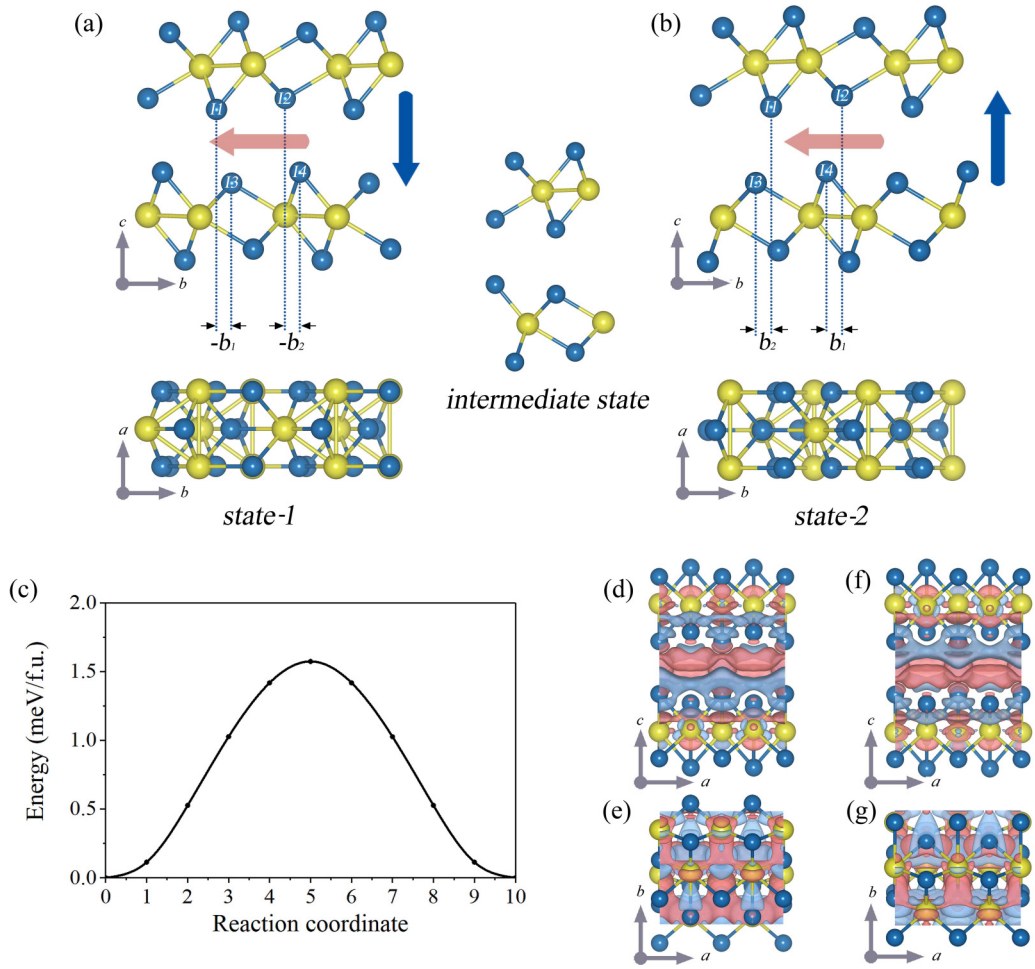

FIG. 3. Out-of-plane ferroelectric switching pathway of bilayer ZrI_2 from (a) *state-1* to (b) *state-2*. Blue and red arrows indicate out-of-plane and in-plane ferroelectric polarization directions, respectively. (c) Energy barrier of 180 ° out-of-plane ferroelectric switching. Differential charge density diagrams of (d) and (e) *state-1* and (f) and (g) *state-2*; red and blue regions represent electron accumulation and depletion, respectively.

ferroelectric switching pathway. The intermediate state during this process has a C_{2v} point group with $\{M_c|0\frac{1}{2}0\}$ symmetry, where M_c is the mirror plane symmetry perpendicular to the c direction and $(0\frac{1}{2}0)$ is half of the lattice translation along the b direction. In this intermediate state, the out-of-plane electric polarization vanishes. To estimate the possibility of the ferroelectric polarization switching pathway, we investigate the energy barrier using the NEB method. As shown in Fig. 3(c), the energy barrier for 180 ° reversing the out-of-plane electric polarization is estimated to be 1.6 meV/f.u., which is larger than that of bilayer WTe_2 (0.6 meV/f.u.) [44]. It should be noted that this barrier for sliding ferroelectricity is the collective barrier where the out-of-plane polarizations of all dipoles must be reversed simultaneously, and it does not correlate to the Curie temperature T_c directly [44]. The Curie temperature for the sliding ferroelectricity in bilayer ZrI_2 depends on the isolated barrier, corresponding to flipping over one dipole while fixing all other surrounding dipoles [44,50,51]. Normally, the in-plane rigidity of 2D materials would result in a large, isolated barrier for sliding ferroelectricity. Note that the Curie temperature for sliding ferroelectricity in bilayer WTe_2 is found to be 350 K experimentally, although its energy barrier is 0.6 meV/f.u. [43,44]. The mechanism of the sliding ferroelectricity in bilayer ZrI_2 is like previous bilayer systems [43,52,53], which thus is experimentally feasible. To simulate the isolated barrier for switching one dipole, we construct an artificial 7×7 supercell containing 588 atoms (Fig. S7(a) in the Supplemental Material [37]), wherein the translation is negative in one unit cell but positive in others. Our NEB calculation shows that the energy barrier for flipping one dipole (with fixing the surrounding dipoles) is 0.06 eV/f.u., as shown in Fig. S7(b) in the Supplemental Material [37]. According to the mean field theory and Heisenberg model [44,54] (see Supplemental Material [37]), the Curie temperature can be roughly estimated to be 476 K. This indicates that the sliding ferroelectricity in bilayer ZrI_2 is feasible and robust.

After reversing the out-of-plane ferroelectric polarization, as shown in Fig. 3(f), the electron gain and loss regions along the c direction are reversed with respect to that of *state-1*. We also find that the in-plane spin textures are reversable upon out-of-plane ferroelectric switching [55] (Fig. S8 in the Supplemental Material [37]). Furthermore, the plane averaged electrostatic potential of *state-2* along the c direction exhibits a negative discontinuity ($\Delta V = -0.03$ eV) between the

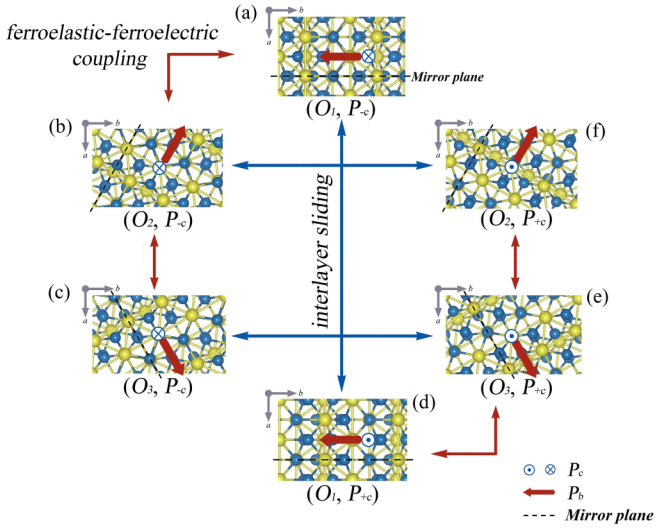

FIG. 4. Schematic diagram of six-logic-state multiferroicity based on the ferroelastic-ferroelectric coupling in bilayer ZrI_2. There are three states with different in-plane polarization when the out-of-plane polarization is (a)–(c) downward or (d)–(f) upward. Red and blue one-way arrows indicate in- and out-of-plane ferroelectric polarization directions, respectively. Red and blue two-way arrows indicate in- and out-of-plane ferroelectric polarization are reversed independently by ferroelastic-ferroelectric coupling and interlayer sliding, respectively.

vacuum levels of the top and bottom layers (Fig. S4(b) in the Supplemental Material [37]). Different from the out-of-plane case, as shown in Fig. 3(g), the in-plane differential charge density along the *b* direction is not reversed. The underlying physics is that *state-2* can be obtained by a mirror operation on *state-1* with respect to the horizontal plane, which does not affect the direction of in-plane electric polarization. This indicates that interlayer sliding is not applicable for realizing in-plane electric switching in bilayer ZrI_2.

Strain tensor (electric polarization vector) is a polar symmetric property tensor of the second rank (first rank). In a ferroelastic (ferroelectric) crystal, polar symmetric property tensors of the second rank (first rank) change with each state shift, but those of the first rank (second rank) are invariable. This fact can be utilized for discerning states of a ferroelastic (ferroelectric) crystal. When the ferroelectricity and ferroelasticity couple with each other, the crystal not only has the characteristics of ferroelectricity and ferroelasticity simultaneously but also has the diagonal effect: change in the polarization vector and change in the strain tensor are accompanied with each other [42]. In detail, both in-plane ferroelectric and ferroelastic switching in bilayer ZrI_2 are essentially linked with the in-plane anisotropy of crystal structure, thus bilayer ZrI_2 harbors the diagonal effect mentioned above. The direction of in-plane ferroelectricity in bilayer ZrI_2 is parallel to the mirror plane M_a. When the arrangement of atoms in bilayer ZrI_2 moves slightly under the ferroelastic switching (Fig. S2 in the Supplemental Material [37]), the lattice structure and mirror plane M_a experience a 120 ° rotation around the *c* axis, which can subsequently cause a 120 ° rotation of the direction of in-plane polarization. Figures 4(a)–4(c) show the crystal structures of the three energetically degenerate, but inequivalent, states with in-plane electric polarization. Obviously, they correspond to O_1, O_2, and O_3 ferroelastic states. Therefore, under external mechanical deformations, the ferroelastic transition process is accompanied with the rotation of the direction of in-plane electric polarization. This suggests that the in-plane electric switching pathway follows the pathway of the tristate ferroelastic switching. The energy barrier for 120 ° reversing the in-plane electric polarization is 0.07 eV/f.u., which suggests the feasibility of in-plane ferroelectricity in bilayer ZrI_2. It thus can be concluded that, with perturbation of the van der Waals interaction, in addition to 2D tristate ferroelasticity, bilayer ZrI_2 exhibits 2D switchable bidirectional ferroelectricity as well.

Figure 2(c) displays the band structure and projected density of states of bilayer ZrI_2. Bilayer ZrI_2 is a semiconductor with an indirect band gap of 0.30 eV. The conduction band minimum (CBM) is located between the Y and M points, while the valence band maximum (VBM) is located between the X and Γ points. From the partial densities of electronic states, the VBM and CBM of bilayer ZrI_2 are mainly contributed by *d* orbitals of Zr atoms and *p* orbitals of I atoms, respectively. Such a semiconducting characteristic would protect the bidirectional ferroelectricity in bilayer ZrI_2 from the annoying electron screening effect induced by metallic properties [56]. The substrate effect on the ferroelectric state is discussed in bilayer WTe_2 experimentally, wherein the substrate is obtained by depositing 15 nm Ti/Au on a SiO_2 surface and does not destabilize the ferroelectric state [57]. As bilayer ZrI_2 exhibits a higher energy barrier and a comparable polarization with respect to bilayer WTe_2, we believe that the ferroelectricity of bilayer ZrI_2 deposited on a suitable substrate can also be detected.

Based on the coexistence of tristate ferroelasticity and bidirectional ferroelectricity in bilayer ZrI_2, we propose a six-logic-state multiferroicity, as shown in Figs. 4(a)–4(f). Here, we refer to out-of-plane ferroelectric polarization along the $+c$ ($-c$) axis as P_{+c} (P_{-c}) and refer to in-plane ferroelectric-ferroelastic polarization states as O_i ($i = 1, 2, 3$). The out-of-plane ferroelectricity and in-plane ferroelectricity-ferroelasticity of bilayer ZrI_2 can be modulated independently. The out-of-plane ferroelectric polarization $P_{\pm c}$ is switchable using interlayer sliding, realizing the transition between the multiferroic states (O_i, P_{+c}) and (O_i, P_{-c}). In experiments, the interlayer sliding could be obtained via external electric field [53], surface friction [58], coherent shear phonon generation [59], and strain-induced interlayer shear [60]. Meanwhile, arising from the in-plane ferroelastic-ferroelectric coupling, ferroelasticity and in-plane ferroelectricity can be switched by 120 ° simultaneously under external mechanical stimulus, achieving the transition among the multiferroic states (O_1, $P_{\pm c}$), (O_2, $P_{\pm c}$), and (O_3, $P_{\pm c}$). Therefore, through the combined effect of external mechanical deformations and interlayer sliding, six distinct logic states can be obtained and switchable, which gives rise to a six-logic-state multiferroicity in bilayer ZrI_2. Considering a strongly anisotropic structure and property in bilayer ZrI_2, these six logic states can be detected directly by measuring the current voltage curve under small bias or measuring polarization-dependent photoluminescence [7,8]. This is of course superior to the conventional

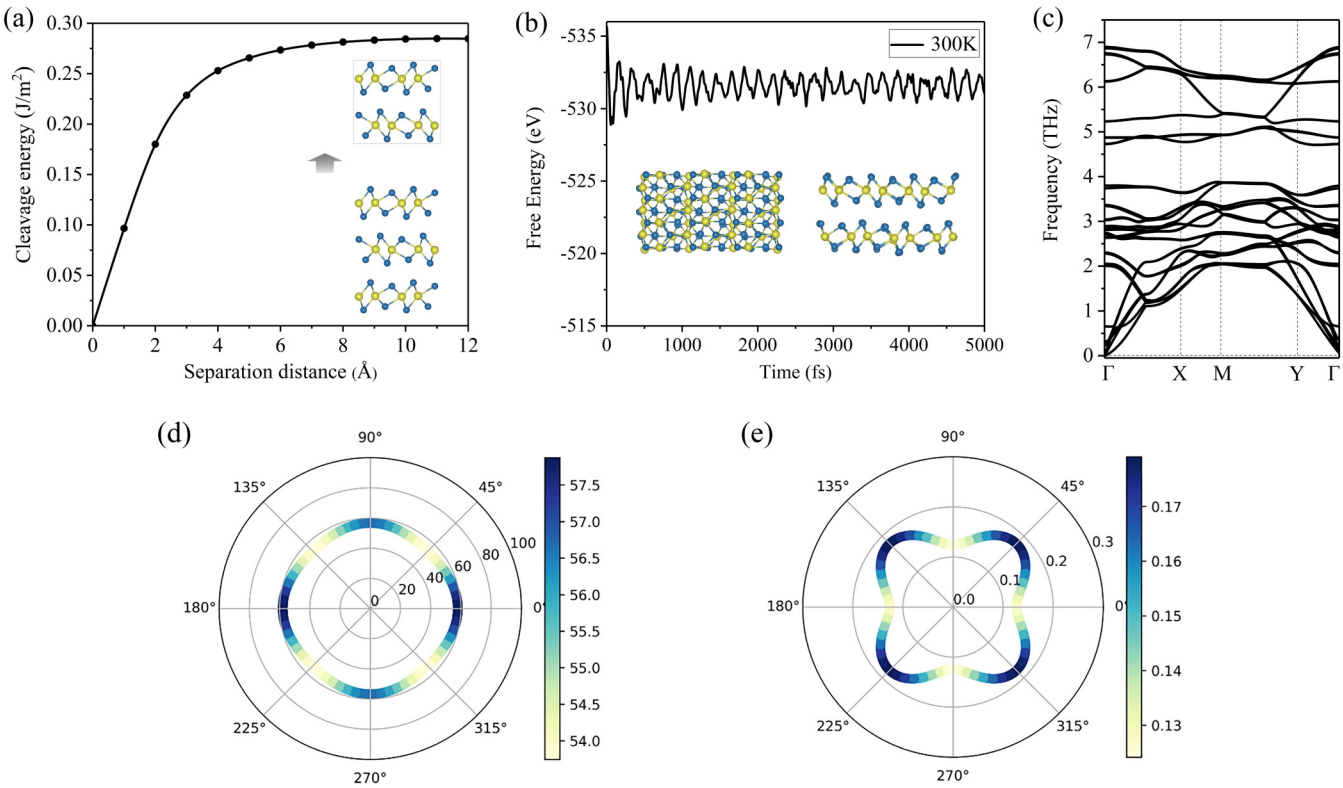

FIG. 5. (a) Cleavage energy varies with separation distance in the process of exfoliating bilayer ZrI_2. Inset in (a) is the schematic diagram of exfoliating a bilayer from five-layer ZrI_2. (b) Variation of total energy of bilayer ZrI_2 at 300 K during *ab initio* molecular dynamics (AIMD) simulations. Inset in (b) is the snapshot taken from the end of the AIMD simulation. (c) Phonon spectra of bilayer ZrI_2. (d) Young's modulus and (e) Poisson's ratio of bilayer ZrI_2 as a function of the angle θ ($\theta = 0^\circ$ corresponds to the a direction).

ferroelastic-ferroelectric multiferroicity in a single-layer lattice that usually shows a four-logic-state multiferroicity, bringing an unprecedented opportunity for exploring high-density multistate data storage.

After confirming the ferroelastic ferroelectricity in bilayer ZrI_2, we investigate its experimental feasibility. Bulk ZrI_2 has been synthesized experimentally [30,31]. Its layered crystal structure facilitates the exfoliation of bilayer ZrI_2. The cleavage energy of bilayer ZrI_2 is estimated to be $0.28\,J/m^2$, comparable with that of $MnPSe_3$ ($0.24\,J/m^2$) [61] and smaller than that of graphene ($0.37\,J/m^2$) [62], as shown in Fig. 5(a). This indicates that bilayer ZrI_2 can readily be exfoliated from the existing bulk through mechanical or liquid exfoliation [63]. To determine the stability of bilayer ZrI_2, we carry out AIMD simulation [Fig. 5(b)]. After heating at 300 K for 5 ps, the geometry of bilayer ZrI_2 is well maintained, implying its thermal stability. Phonon spectra calculation is further performed to confirm its stability. As shown in Fig. 5(c), the absence of imaginary vibrational frequencies within the entire Brillouin zone reveals that bilayer ZrI_2 is dynamically stable. In addition, we calculate its elastic constants, which are found to be $C_{11} = 124\,N/m$, $C_{22} = 128\,N/m$, $C_{12} = 16\,N/m$, and $C_{66} = 48\,N/m$. The elastic constants obey the Born criteria: $C_{11}C_{22} - {C_{12}}^2 > 0$ and $C_{66} > 0$ [64,65], indicating that bilayer ZrI_2 is mechanically stable. Given the elastic constants, the Young's modulus and Poisson's ratio of bilayer ZrI_2 along the in-plane θ are presented in Figs. 5(d) and 5(e) [15,66–70]. Details are reported in the Supplemental Material [37]. These facts enable that the interesting phenomenon discussed above can be readily obtained in experiment.

At last, we discuss the feasibility of ferroelastic-ferroelectric multiferroics in other bilayer systems. As we mentioned above, to design or search for 2D ferroelastic-ferroelectric multiferroics, the single-layer candidates selected here must exhibit ferroelasticity, as ferroelasticity is stubborn. To this end, we could narrow down our choice to the existing single-layer ferroelastic materials [3,4,7,15–17,71]. In addition, for introducing electric polarization using the van der Waals interaction as perturbation, the charge distribution of the materials should be sensitive to interlayer stacking. To satisfy this condition, we could focus on multicomponent compounds. Following this design principle, 2D ferroelastic-ferroelectric multiferroics exist extensively in a bilayer lattice, such as BN, AlN, GaN, ZnO, MoS_2, 1T′-WTe_2, 1T′-$MoTe_2$, etc. We wish to stress that the energy barrier for the ferroelastic-ferroelectric switching is a key ingredient which decides whether the ferroelastic-ferroelectric multiferroics are practical or not. Overall, we suggest that this scheme could extensively expand the scope of material candidates for 2D ferroelastic-ferroelectric multiferroics.

In conclusion, we demonstrate a design principle for achieving 2D ferroelastic-ferroelectric multiferroics using the van der Waals interaction as perturbation in a bilayer lattice. Based on first-principles calculations, an example system of

bilayer ZrI_2 is shown to harbor 2D ferroelastic ferroelectricity. In this system, the ferroelasticity stems from the spontaneous structure polarization, and the in- and out-of-plane ferroelectric polarizations result from interlayer charge redistribution. The out-of-plane ferroelectric polarization associates with interlayer sliding, while the in-plane ferroelectric polarization relates to ferroelastic switching. Based on the coexistence of ferroelasticity and out-of-plane–in-plane ferroelectricity, a promising six-logic-state multiferroicity is proposed. This design scheme is not restricted to bilayer ZrI_2 but also can be applied to other bilayer lattices. Our results reveal the existence of ferroelastic-ferroelectric multiferroicity in a bilayer lattice and offers a platform for exploring 2D ferroelastic-ferroelectric multiferroics.

ACKNOWLEDGMENTS

This paper is supported by the National Natural Science Foundation of China (No. 11804190 and No. 12074217), Shandong Provincial Natural Science Foundation (No. ZR2019QA011 and No. ZR2019MEM013), Shandong Provincial Key Research and Development Program (Major Scientific and Technological Innovation Project; No. 2019JZZY010302), Shandong Provincial Key Research and Development Program (No. 2019RKE27004), Shandong Provincial Science Foundation for Excellent Young Scholars (No. ZR2020YQ04), Qilu Young Scholar Program of Shandong University, and Taishan Scholar Program of Shandong Province.

[1] C. Gong, L. Li, Z. Li, H. Ji, A. Stern, Y. Xia, T. Cao, W. Bao, C. Wang, Y. Wang, Z. Q. Qiu, R. J. Cava, S. G. Louie, J. Xia, and X. Zhang, Discovery of intrinsic ferromagnetism in two-dimensional van der Waals crystals, Nature **546**, 265 (2017).

[2] A. Belianinov, Q. He, A. Dziaugys, P. Maksymovych, E. Eliseev, A. Borisevich, A. Morozovska, J. Banys, Y. Vysochanskii, and S. V. Kalinin, $CuInP_2S_6$ room temperature layered ferroelectric, Nano Lett. **15**, 3808 (2015).

[3] L. Seixas, A. S. Rodin, A. Carvalho, and A. H. Castro Neto, Multiferroic Two-Dimensional Materials, Phys. Rev. Lett. **116**, 206803 (2016).

[4] W. Li and J. Li, Ferroelasticity and domain physics in two-dimensional transition metal dichalcogenide monolayers, Nat. Commun. **7**, 10843 (2016).

[5] B. Huang, G. Clark, E. Navarro-Moratalla, D. R. Klein, R. Cheng, K. L. Seyler, D. Zhong, E. Schmidgall, M. A. Mcguire, D. H. Cobden, W. Yao, D. Xiao, P. Jarillo-Herrero, and X. Xu, Layer-dependent ferromagnetism in a van der Waals crystal down to the monolayer limit, Nature **546**, 270 (2017).

[6] J. Lado and J. Fernández-Rossier, On the origin of magnetic anisotropy in two dimensional CrI_3, 2D Mater. **4**, 035002 (2017).

[7] M. Wu and X. Zeng, Intrinsic ferroelasticity and/or multiferroicity in two-dimensional phosphorene and phosphorene analogues, Nano Lett. **16**, 3236 (2016).

[8] H. Wang, X. Li, J. Sun, Z. Liu, and J. Yang, BP_5 monolayer with multiferroicity and negative Poisson's ratio: A prediction by global optimization method, 2D Mater. **4**, 045020 (2017).

[9] M. Wu and X. Zeng, Bismuth oxychalcogenides: A new class of ferroelectric/ferroelastic materials with ultra high mobility, Nano Lett. **17**, 6309 (2017).

[10] H. Wang and X. Qian, Two-dimensional multiferroics in monolayer group IV monochalcogenides, 2D Mater. **4**, 015042 (2017).

[11] S.-H. Zhang and B.-G. Liu, A controllable robust multiferroic GaTeCl monolayer with colossal 2D ferroelectricity and desirable multifunctionality, Nanoscale **10**, 5990 (2018).

[12] Y. Gao, M. Wu, and X. Zeng, Phase transitions and ferroelasticity multiferroicity in bulk and two-dimensional silver and copper monohalides, Nanoscale Horiz. **4**, 1106 (2019).

[13] N. Hill, Why are there so few magnetic ferroelectrics? J. Phys. Chem. B **104**, 6694 (2000).

[14] B. Xu, S. Li, K. Jiang, J. Yin, Z. Liu, Y. C. Cheng, and W. Zhong, Switching of the magnetic anisotropy via strain in two dimensional multiferroic materials: CrSX (X = Cl, Br, I), Appl. Phys. Lett. **116**, 052403 (2020).

[15] Y. Ma, L. Kou, B. Huang, Y. Dai, and T. Heine, Two-dimensional ferroelastic topological insulators in single-layer Janus transition metal dichalcogenides MSSe (M = Mo, W), Phys. Rev. B **98**, 085420 (2018).

[16] J.-H. Yuan, G.-Q. Mao, K.-H. Xue, J. Wang, and X.-S. Miao, A new family of two-dimensional ferroelastic semiconductors with negative Poisson's ratios, Nanoscale **12**, 14150 (2020).

[17] L. Zhou, Z. Zhuo, L. Kou, A. Du, and S. Tretiak, Computational dissection of two-dimensional rectangular titanium mononitride TiN: Auxetics and promises for photocatalysis, Nano Lett. **17**, 4466 (2017).

[18] Y. Wang, C. Xiao, M. Chen, C. Hu, J. Zou, C. Wu, J. Jiang, S. A. Yang, Y. Lu, and W. Ji, Two-dimensional ferroelectricity and switchable spin-textures in ultra-thin elemental Te multilayers, Mater. Horiz. **5**, 521 (2018).

[19] W. Ding, J. Zhu, Z. Wang, Y. Gao, D. Xiao, Y. Gu, Z. Zhang, and W. Zhu, Prediction of intrinsic two-dimensional ferroelectrics in In_2Se_3 and other III_2-VI_3 van der Waals materials, Nat. Commun. **8**, 14956 (2017).

[20] G. Kresse and J. Furthmüller, Efficient iterative schemes for *ab initio* total-energy calculations using a plane-wave basis set, Phys. Rev. B **54**, 11169 (1996).

[21] J. P. Perdew, K. Burke, and M. Ernzerhof, Generalized Gradient Approximation Made Simple, Phys. Rev. Lett. **77**, 3865 (1996).

[22] G. Kresse and D. Joubert, From ultrasoft pseudopotentials to the projector augmented-wave method, Phys. Rev. B **59**, 1758 (1999).

[23] S. Grimme, S. Ehrlich, and L. Goerigk, Effect of the damping function in dispersion corrected density functional theory, J. Comput. Chem. **32**, 1456 (2011).

[24] R. N. Barnett and U. Landman, Born-Oppenheimer molecular-dynamics simulations of finite systems: Structure and dynamics of $(H_2O)_2$, Phys. Rev. B **48**, 2081 (1993).

[25] A. Togo, F. Oba, and I. Tanaka, First-principles calculations of the ferroelastic transition between rutile-type and $CaCl_2$-type SiO_2 at high pressures, Phys. Rev. B **78**, 134106 (2008).

[26] G. Mills, H. Jónsson, and G. K. Schenter, Reversible work transition state theory: Application to dissociative adsorption of hydrogen, Surf. Sci. **324**, 305 (1995).

[27] R. D. King-Smith and D. Vanderbilt, Theory of polarization of crystalline solids, Phys. Rev. B **47**, 1651 (1993).

[28] S. N. Shirodkar and U. V. Waghmare, Emergence of Ferroelectricity at a Metal-Semiconductor Transition in a 1T Monolayer of MoS_2, Phys. Rev. Lett. **112**, 157601 (2014).

[29] C. Huang, Y. Du, H. Wu, H. Xiang, K. Deng, and E. Kan, Prediction of Intrinsic Ferromagnetic Ferroelectricity in a Transition-Metal Halide Monolayer, Phys. Rev. Lett. **120**, 147601 (2018).

[30] D. H. Guthrie and J. D. Corbett, Synthesis and structure of an infinite-chain form of ZrI_2 (α), J. Solid State Chem. **37**, 256 (1981).

[31] J. D. Corbett and D. H. Guthrie, A second infinite-chain form of zirconium diiodide (β) and its coherent intergrowth with α-zirconium diiodide, Inorg. Chem. **21**, 1747 (1982).

[32] S. W. Depner, N. D. Cultrara, K. E. Farley, Y. Qin, and S. Banerjee, Ferroelastic domain organization and precursor control of size in solution-grown hafnium dioxide nanorods, ACS Nano **8**, 4678 (2014).

[33] A. V. Virkar and R. L. Matsumoto, Ferroelastic domain switching as a toughening mechanism in tetragonal zirconia, J. Am. Ceram. Soc. **69**, 224 (1986).

[34] V. Anbusathaiah, S. Jesse, M. A. Arredondo, F. C. Kartawidjaja, O. S. Ovchinnikov, J. Wang, S. V. Kalinin, and V. Nagarajan, Ferroelastic domain wall dynamics in ferroelectric bilayers, Acta Mater. **58**, 5316 (2010).

[35] G. F. Nataf and M. Guennou, Optical studies of ferroelectric and ferroelastic domain walls, J. Phys.: Condens. Matter **32**, 183001 (2020).

[36] J. Britson, C. Nelson, X. Pan, and L.-Q. Chen, First-order morphological transition of ferroelastic domains in ferroelectric thin films, Acta Mater. **75**, 188 (2014).

[37] See Supplemental Material at http://link.aps.org/supplemental/10.1103/PhysRevB.103.165420 for Figs. S1–S8 and detailed description of dependence of energy and out-of-plane polarization of bilayer ZrI_2 on interlayer displacement along the b direction; energy barrier for flipping one dipole of bilayer ZrI_2; the Young's modulus and Poisson's ratio of bilayer ZrI_2.

[38] L. Kou, Y. Ma, C. Tang, Z. Sun, A. Du, and C. Chen, Ferroelastic borophane: A novel 2D material with negative Poisson's ratio and switchable Dirac transport channels, Nano Lett. **16**, 7910 (2016).

[39] O. Kanert, H. Schulz, and J. Albers, Nuclear magnetic resonance study of the cubic-to-tetragonal phase transition in $BaTiO_3$, Solid State Commu. **91**, 465 (1994).

[40] A. Leschhorn and H. Kliem, A feedback model for relaxors, Ferroelectrics **553**, 8 (2019).

[41] R. Fei, W. Kang, and L. Yang, Ferroelectricity and Phase Transitions in Monolayer Group-IV Monochalcogenides, Phys. Rev. Lett. **117**, 097601 (2016).

[42] K. Aizu, Possible species of "ferroelastic" crystals and of simultaneously ferroelectric and ferroelastic crystals, J. Phys. Soc. Jpn. **27**, 387 (1969).

[43] Z. Fei, W. Zhao, T. A. Palomaki, B. Sun, M. K. Miller, Z. Zhao, J. Yan, X. Xu, and D. H. Cobden, Ferroelectric switching of a two-dimensional metal, Nature **560**, 336 (2018).

[44] Q. Yang, M. Wu, and J. Li, Origin of two-dimensional vertical ferroelectricity in WTe_2 bilayer and multilayer, J. Phys. Chem. Lett. **9**, 7160 (2018).

[45] H. Wieder, Electrical behavior of barium titanatge single crystals at low temperatures, Phys. Rev. **99**, 1161 (1955).

[46] B. Meyer and D. Vanderbilt, *Abinitio* study of $BaTiO_3$ and $PbTiO_3$ surfaces in external electric fields, Phys. Rev. B **63**, 205426 (2001).

[47] E. Bruyer, D. D. Sante, B. Barone, A. Stroppa, M.-H. Whangbo, and S. Picozzi, Possibility of combining ferroelectricity and Rashba-like spin splitting in monolayers of the 1T-type transition-metal dichalcogenides MX_2 (M = Mo, W; $X = S$, Se, Te), Phys. Rev. B **94**, 195402 (2016).

[48] A. Chandrasekaran, A. Mishra, and A. K. Singh, Ferroelectricity, antiferroelectricity, and ultrathin 2D electron/hole gas in multifunctional monolayer MXene, Nano Lett. **17**, 3290 (2017).

[49] S. Shen, X. Xu, B. Huang, L. Kou, Y. Dai, and Y. Ma, Intrinsic triferroicity in a two-dimensional lattice, Phys. Rev. B **103**, 144101 (2021).

[50] M. Wu, T. Duan, C. Lu, H. Fu, S. Dong, and J. Liu, Proton transfer ferroelectricity/multiferroicity in rutile oxyhydroxides, Nanoscale **10**, 9509 (2018).

[51] M. Wu, X. C. Zeng, and P. Jena, Unusual magnetic properties of functionalized graphene nanoribbons, J. Phys. Chem. Lett. **4**, 2482 (2013).

[52] L. Li and M. Wu, Binary compound bilayer and multilayer with vertical polarizations: Two-dimensional ferroelectrics, multiferroics, and nanogenerators, ACS Nano **11**, 6382 (2017).

[53] J. Xiao, Y. Wang, H. Wang, C. D. Pemmaraju, S. Wang, P. Muscher, E. J. Sie, C. M. Nyby, T. P. Devereaux, X. Qian, X. Zhang, and A. M. Lindenberg, Berry curvature memory through electrically driven stacking transitions, Nat. Phys. **16**, 1028 (2020).

[54] M. Wu, Z. Wang, J. Liu, W. Li, H. Fu, L. Sun, X. Liu, M. Pan, H. Weng, and M. Dincă, Conetronics in 2D metal-organic frameworks: Double/half Dirac cones and quantum anomalous Hall effect, 2D Mater. **4**, 015015 (2017).

[55] Z. Lin, C. Si, S. Duan, C. Wang, and W. Duan, Rashba splitting in bilayer transition metal dichalcogenides controlled by electronic ferroelectricity, Phys. Rev. B **100**, 155408 (2019).

[56] W. Luo, K. Xu, and H. Xiang, Two-dimensional hyperferroelectric metals: A different route to ferromagnetic-ferroelectric multiferroics, Phys. Rev. B **96**, 235415 (2017).

[57] P. Sharma, F.-X. Xiang, D. F. Shao, D. Zhang, E. Y. Tsymbal, A. R. Hamilton, and J. Seidel, A room-temperature ferroelectric semimetal, Sci. Adv. **5**, eaax5080 (2019).

[58] J. Quereda, A. Castellanos-Gomez, N. Agraït, and G. Rubio-Bollinger, Single-layer MoS_2 roughness and sliding friction quenching by interaction with atomically flat substrates, Appl. Phys. Lett. **105**, 053111 (2014).

[59] O. Matsuda, O. B. Wright, D. H. Hurley, V. E. Gusev, and K. Shimizu, Coherent Shear Phonon Generation and Detection with Ultrashort Optical Pulses, Phys. Rev. Lett. **93**, 095501 (2004).

[60] J.-U. Lee, S. Woo, J. Park, H. C. Park, Y.-W. Son, and H. Cheong, Strain-shear coupling in bilayer MoS_2, Nat. Commun. **8**, 1370 (2017).

[61] X. Li, X. Wu, and J. Yang, Half-metallicity in $MnPSe_3$ exfoliated nanosheet with carrier doping, J. Am. Chem. Soc. **136**, 11065 (2014).

[62] T. Björkman, A. Gulans, A. V. Krasheninnikov, and R. M. Nieminen, van der Waals Bonding in Layered Compounds from Advanced Density-Functional First-Principles Calculations, Phys. Rev. Lett. **108**, 235502 (2012).

[63] M. Qiao, J. Liu, Y. Wang, Y. Li, and Z. Chen, $PdSeO_3$ monolayer: Promising inorganic 2D photocatalyst for direct overall water splitting without using sacrificial reagents and cocatalysts, J. Am. Chem. Soc. **140**, 12256 (2018).

[64] Y. Wang, M. Qiao, Y. Li, and Z. Chen, A two-dimensional CaSi monolayer with quasi-planar pentacoordinate silicon, Nanoscale Horiz. **3**, 327 (2018).

[65] J. Wang, S. Yip, S. R. Phillpot, and D. Wolf, Crystal Instabilities at Finite Strain, Phys. Rev. Lett. **71**, 4182 (1993).

[66] E. Cadelano, P. L. Palla, S. Giordano, and L. Colombo, Elastic properties of hydrogenated graphene, Phys. Rev. B **82**, 235414 (2010).

[67] R. Peng, Y. Ma, Z. He, B. Huang, L. Kou, and Y. Dai, Single-layer Ag_2S: A two-dimensional bidirectional auxetic semiconductor, Nano Lett. **19**, 1227 (2019).

[68] R. C. Andrew, R. E. Mapasha, A. M. Ukpong, and N. Chetty, Mechanical properties of graphene and boronitrene, Phys. Rev. B **85**, 125428 (2012).

[69] K. H. Michel and B. Verberck, Theory of elastic and piezoelectric effects in two-dimensional hexagonal boron nitride, Phys. Rev. B **80**, 224301 (2009).

[70] Z. Gao, X. Dong, N. Li, and J. Ren, Novel two-dimensional silicon dioxide with in-plane negative Poisson's ratio, Nano Lett. **17**, 772 (2017).

[71] Z. Tu and M. Wu, Ultrahigh-strain ferroelasticity in two-dimensional honeycomb monolayers: From covalent to metallic bonding, Sci. Bull. **65**, 147 (2020).